ChemComm

ROYAL SOCIETY OF CHEMISTRY

COMMUNICATION

View Article Online
View Journal | View Issue

Open Access Article. Published on 14 April 2020. Downloaded on 12/4/2025 8:25:43 PM.
This article is licensed under a Creative Commons Attribution-NonCommercial 3.0 Unported Licence.

Check for updates

Cite this: *Chem. Commun.*, 2020, **56**, 5405

Received 21st January 2020,
Accepted 20th March 2020

DOI: 10.1039/d0cc00579g

rsc.li/chemcomm

A mitochondria-targeting NIR fluorescent potassium ion sensor: real-time investigation of the mitochondrial K^+ regulation of apoptosis *in situ*†

Guangjie Song,[ab] Di Jiang,[b] Lei Wang,[a] Juewei Ning,[a] Xiangzhong Sun,[a] Fengyu Su,*[c] Meiwan Chen*[b] and Yanqing Tian *[a]

The first NIR fluorescent mitochondria-targeting K^+ sensor, denoted as TAC-Rh, was developed. The produced sensor consists of a rhodamine analog as the fluorophore and triazacryptand (TAC) as the K^+ recognition unit. Compared to the K^+ sensors reported previously, TAC-Rh exhibits two unique optical properties: the largest Stokes shifts (120 nm) and the longest emission peak wavelength (720 nm). With the assistance of this novel sensor, real-time changes of K^+ concentrations in mitochondria during apoptosis were monitored for the first time. Moreover, it was also the first time that the relationship between mitochondrial K^+ flux and apoptosis was investigated in real time using fluorescence imaging.

The potassium ion (K^+) is one of the predominant ions in living cells (about 150 mM), and is closely involved in many biological processes, such as kidney function, nerve transmission, heart beat and muscle contraction.[1] Yu *et al.* first proposed an association between apoptosis and the loss of intracellular potassium ions.[2] In 2016, Vodnala *et al.* discovered that an increase in the concentration of K^+ in tumor microenvironments could reduce the activity of T cells and prevent their anti-tumor function,[3] and discovered in 2019 that an increased concentration of K^+ would also destroy T cell metabolism and nutrient uptake, leading to a starvation state known as autophagy.[4] These discoveries opened up new avenues for developing therapies aimed at mobilizing the immune system against cancer, with these efforts involving exploring the role of K^+ in these processes. Therefore, determination of intracellular potassium levels is essential.

More and more studies have found mitochondria to be involved in a variety of key events involving the regulation of apoptosis.[5,6] However, most of these studies did not delve deeply into the organelle level to explore the relationship between mitochondrial K^+ and apoptosis due to the lack of appropriate tools. Therefore, constructing a tool to trace in real time the flow of K^+ in mitochondria would be expected to be very beneficial for analyzing the relationship between mitochondrial K^+ and apoptosis.

In previous measurements of mitochondrial K^+ concentration, it was usually necessary to isolate mitochondria, a complex process not feasible for determining the concentration of mitochondrial K^+ in real time.[7] Confocal laser scanning microscopy has turned out to be an important tool for understanding the biological states of metal ions, and doing so in a damage-free manner with high time-space resolution.[8] However, currently, only a few K^+ sensors have been prepared.[9] Moreover, **PBFI**, the most common potassium indicator, was reported to be interfered with by sodium to some extent.[10] Since He *et al.* first reported a K^+ sensor using a highly selective triazacryptand (**TAC**) ligand as the K^+-sensing moiety,[11] a few **TAC**-derived K^+ sensors were further developed and used for intracellular imaging of K^+.[9c,e,g,12]

The emissions of most fluorescent sensors have been observed to occur in the ultraviolet visible (UV/Vis) range (400–700 nm in wavelength), leading to light-induced toxicity, and weak tissue penetration and resolution, when applied *in vivo* due to the auto fluorescence and light absorption of biomolecules. It would be preferable to pursue low-energy NIR fluorescent sensors to minimize light-induced toxicity, to lower the level of interference from biomolecules, and deepen tissue penetration.[13] However, the fluorophores used for K^+ sensors, including boron dipyrromethenes (BODIPYs),[9f,14] naphthalimides,[9g,15] and other dyes,[9b,16] have emission wavelengths below 600 nm. So far, only four K^+ fluorescent sensors with emission wavelengths of over 600 nm have been reported (Zhou *et al.*, 2011, $\lambda_{max\,em}$ = 650 nm;[9c] Sui *et al.*, 2015, $\lambda_{max\,em}$ = 650 nm;[9e] Müller *et al.*, 2016, $\lambda_{max\,em}$ = 688 nm;[9d] Bandara *et al.*, 2017, $\lambda_{max\,em}$ = 680 nm[17]) (see Table S1 in ESI†). Although these fluorescence emission wavelengths are partly situated in the NIR region (700–900 nm in wavelength), the peaks of all these fluorescence emissions are at wavelengths of shorter than 700 nm.

[a] *Department of Materials Science and Engineering Southern University of Science and Technology, Shenzhen, 518055, China. E-mail: tianyq@sustech.edu.cn*
[b] *State Key Laboratory of Quality Research in Chinese Medicine Institute of Chinese Medical Sciences, University of Macau, Macao 999078, China. E-mail: mwchen@umac.mo*
[c] *Academy for Advanced Interdisciplinary Studies Southern University of Science and Technology, Shenzhen, 518055, China. E-mail: fysu@sustech.edu.cn*

† Electronic supplementary information (ESI) available: Synthesis, additional methods, and figures (Fig. S1–S21). See DOI: 10.1039/d0cc00579g

Open Access Article. Published on 14 April 2020. Downloaded on 12/4/2025 8:25:43 PM.
This article is licensed under a Creative Commons Attribution-NonCommercial 3.0 Unported Licence.

Ideal intracellular K^+ sensors should display the following characteristics:[18] long-wavelength fluorescence, wide dynamic K^+ detection range (100–300 mM), insensitivity to Na^+ (5–15 mM in intracellular fluid) and other metal ions at physiological concentrations, pH insensitivity, and rapid response. Our strategy was to integrate **TAC** for K^+ recognition with a rhodamine analog as an NIR fluorophore. Herein, **TAC-Rh** with a K^+ detection range of 16 to 400 mM was designed and synthesized, enabling its suitable application for sensing intracellular K^+. **TAC-Rh** is the first NIR fluorescent K^+ sensor with a peak of emission wavelength of up to 720 nm, a value greater than those of all fluorescent K^+ sensors reported to date. And **TAC-Rh** in HEPES buffer shows a Stokes shift of 120 nm, also a value larger than those of all reported potassium ion sensors. In addition, **TAC-Rh** with its positive charge preferentially accumulated in mitochondria, realizing *in situ* monitoring of mitochondrial K^+ concentration. To date, only two mitochondrion-targeting K^+ sensors with short emission wavelengths have been reported by us.[9h,12] And the sensors were only used to observe the fluxes of K^+ in mitochondria, and were not used for exploring mitochondrial K^+ regulation of apoptosis. In this work, the optical properties of **TAC-Rh** and its applications in studying the relationship between mitochondrial potassium concentration and apoptosis were investigated.

Fig. 1a shows the synthetic route to **TAC-Rh**. In brief, **TAC-Rh** was obtained by forming a covalent C=C bonds between **TAC** and the rhodamine analog, in turn achieved by carrying out a condensation reaction of **TAC-CHO**[9c] with compound **1** in an acetic anhydride solution. And the structure of **TAC-Rh** was characterized by performing ^{1}H NMR spectroscopy and high-resolution mass spectroscopy (Fig. S1 and S2, ESI†).

Due to the electrostatic interaction resulting from the positively charged cationic **TAC-Rh** and negative transmembrane potential of mitochondria, most of the **TAC-Rh** was expected to localize in the mitochondria.[19] In the structure of the **TAC-Rh** molecule, the tertiary amino group of TAC acted as an electron donor and the rhodamine analog fluorophore served as an electron acceptor. The fluorescence quenching effect took place due to the photo-induced electron transfer (PET) (Fig. 1b) from TAC to the rhodamine analog. As a result, **TAC-Rh** in free form displayed weak emission, while a significant fluorescence intensity increase occurred upon the addition of K^+ because the complexation between TAC and K^+ effectively inhibited the fluorescence quenching from PET. Absorption and fluorescence titration experiments of **TAC-Rh** in a HEPES buffer containing centrimonium bromide (CTAB) as a surfactant, which can increase the solubility of the probe, were performed at various K^+ concentrations. The acquired UV spectra of the **TAC-Rh**–K^+ complex show a stronger UV absorption than that of the free **TAC-Rh** after the addition of K^+ (Fig. S3, ESI†). As exhibited in Fig. 2a and b, a remarkable fluorescence response at 720 nm was observed with an excitation wavelength of 600 nm, and the fluorescence response of **TAC-Rh** showed a linear relationship to log[K^+] in the range 16–400 mM. The K_d value was determined using the Benesi–Hildebrand plot to be 105 mM (Fig. S3b, ESI†),[9c] indicating the suitability of using **TAC-Rh** for monitoring intracellular K^+ levels.

Any intracellular K^+ sensor should be designed to be insensitive to other metal ions at their intracellular physiological levels. Therefore, the fluorescence changes for **TAC-Rh** were tested in the presence of the following intracellular cations at their respective physiological concentrations: Cu^{2+} (50 μM), Ca^{2+} (2 mM), Mg^{2+} (2 mM), Mn^{2+} (50 μM), Fe^{3+} (50 μM), Fe^{2+} (50 μM),

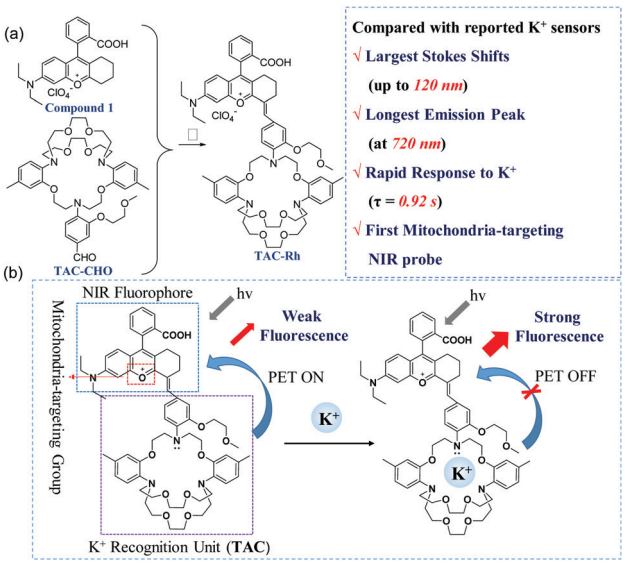

Fig. 1 Rational design, synthetic route (a), and proposed PET process (b) for **TAC-Rh**; I: acetic anhydride, 90 °C, 8 h.

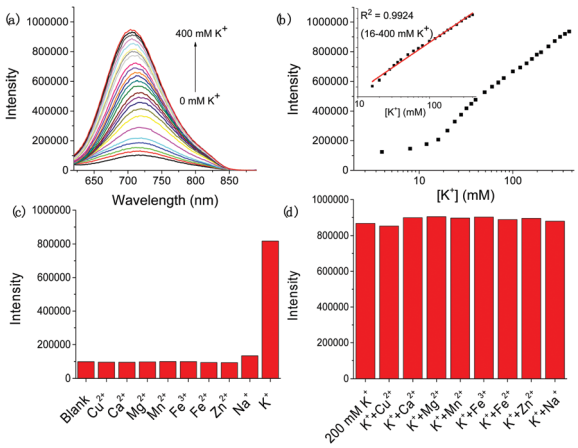

Fig. 2 Fluorescence titration spectra produced by gradually adding KCl at concentrations from 0 to 400 mM to a solution of **TAC-Rh** (10 μM) in HEPES/HCl buffer (pH 7.4, 5.0 mM)/CTAB (0.5 mM) and exciting the solutions with light of a wavelength of 600 nm (a). Plot of the fluorescence intensity of **TAC-Rh** at 720 nm *versus* K^+ concentration. The inset shows the relationship between the fluorescence intensity and K^+ concentration at concentrations between 16 and 400 mM and a fit of a line to these data (R^2 = 0.9924) (b). Fluorescence intensities at 720 nm of various solutions of **TAC-Rh** (10 μM) containing different metal cations in HEPES buffer (pH 7.4, 5.0 mM)/CTAB (0.5 mM) (c). Fluorescence intensities at 720 nm of various solutions of the **TAC-Rh**–K^+ (200 mM) complex containing other metal cations. The ions were from $CuCl_2$ (50 μM), $CaCl_2$ (2 mM), $MgCl_2$ (2 mM), $MnCl_2$ (50 μM), $FeCl_3$ (50 μM), $FeCl_2$ (50 μM), $ZnCl_2$ (2 mM), NaCl (15 mM), and KCl (200 mM), *i.e.*, all of them at their respective intracellular physiological concentrations (d).

Open Access Article. Published on 14 April 2020. Downloaded on 12/4/2025 8:25:43 PM.
This article is licensed under a Creative Commons Attribution-NonCommercial 3.0 Unported Licence.

Zn^{2+} (2 mM), Na^+ (15 mM), and K^+ (150 mM). The results indicated that **TAC-Rh** showed little response to any of the other intracellular cations (Fig. 2c), and it responded to K^+ without interference in the presence of any of the above cations (Fig. 2d). The fluorescence intensities of **TAC-Rh** and **TAC-Rh**–K^+ were also insensitive to pH over the range pH 5.0–9.0 (Fig. S4, ESI†). Notably, a remarkable fluorescence turn-on response was observed almost immediately after adding of K^+, revealing the rapid response of **TAC-Rh** to K^+ ($\tau_{95\%}$ = 0.92 s) (Fig. S5, ESI†).

Based on the above satisfactory photophysical properties of **TAC-Rh** in sensing K^+, it was further applied to track potassium fluxes in live cells (HeLa cells, MCF7 cells, and MDA-MB-231 cells) by recording fluorescence intensities in real time. The cytotoxicity of **TAC-Rh** towards HeLa, MCF7 and MDA-MB-231 cells was first assessed by performing the 3-(4,5-dimethyl-2-thiazolyl)-2,5-diphenyl-2-*H*-tetrazolium bromide (thiazolyl blue tetrazolium bromide, MTT)-based colorimetric assay. After being incubated with **TAC-Rh** at a concentration of 3 μM for 2 h, the viability of each of the three cell lines was over 95% (Fig. S8, ESI†), suggesting that **TAC-Rh** had no marked cytotoxicity toward the three cell lines under these experimental conditions.

The ability of **TAC-Rh** to target mitochondria was then assessed by evaluating the colocalization of **TAC-Rh** using MitoTracker Green (MTG, a commercial mitochondrial marker). The results showed that **TAC-Rh** mainly localized in mitochondria with a Mander's overlap co-efficiency of 0.94 (Fig. 3).

After the demonstration of the specific colocalization of **TAC-Rh** in mitochondria, **TAC-Rh** was used to monitor mitochondrial K^+ fluxes. Three kinds of cells (HeLa, MCF7 and MDA-MB-231 cells) internalized with **TAC-Rh** (3 μM) for 30 min were treated with ionomycin or nigericin, which can effectively induce K^+ efflux. The intensity of the fluorescence of **TAC-Rh** in the single ionomycin or nigericin groups significantly decreased within 2 min, as did the rate of efflux of mitochondrial K^+ (Fig. S12–S19, ESI†). While as a control, fluorescence signals in all three of these cells without any treatment showed relatively small decreases in 10 min (Fig. S9–S11, ESI†). Furthermore, mitochondrial K^+ effluxes could be obviously delayed by treating the cells with ionomycin/nigericin in an extracellular environment having a high concentration of K^+, which was supposed to have an inhibitory effect on potassium ion efflux owing to the decreased [K^+] gradient between the insides and outsides of the mitochondria. Delayed mitochondrial K^+ efflux was observed in the ionomycin- or nigericin-treated groups when the cells in culture medium containing high concentrations of K^+ compared those containing a normal concentration of K^+ (Fig. S12–S19, ESI†). The above phenomenon indicated that **TAC-Rh** can respond in real time to mitochondrial K^+ levels *via* fluorescence intensity changes.

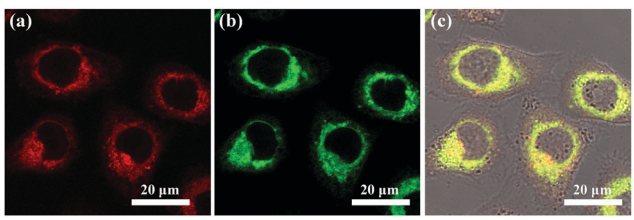

Fig. 3 Confocal fluorescence microscope images of HeLa cells co-stained with MitoTracker Green FM and **TAC-Rh** (3 μM). Red emission from **TAC-Rh** (a). Green emission from MitoTracker Green FM (b). Overlay of MitoTracker Green and **TAC-Rh** (c). Excitation filter: 638 nm for **TAC-Rh**, 488 nm for Mito-Tracker Green. Emission: 650–750 nm for **TAC-Rh**, 500–550 nm for Mito-Tracker Green.

D'Mello *et al.* pointed out that the depletion of potassium ions induced by ionomycin in cells could lead to cell shrinkage, activation of caspases, and DNA breakage, and finally cell apoptosis.[20] In this work, besides the observation of ionomycin-induced mitochondrial K^+ efflux by the designed sensor **TAC-Rh**, annexin V/FITC-PI staining was simultaneously performed to *in situ* monitor the apoptosis process. The results showed that along with the markedly decreased fluorescence intensity of **TAC-Rh** within 10 min of treatment with ionomycin (Fig. 4a and c), the fluorescence signal of annexin V/FITC indicating early-stage apoptosis gradually strengthened. And the typical characteristics of cell apoptosis including cell shrinkage and membrane blebbing were observed in the bright field, but the positive PI signals indicating late-stage apoptosis or dead cells did not appear until ~30 min of treatment with ionomycin. The results indicated that mitochondrial K^+ efflux and early-stage apoptosis occurred almost simultaneously in the presence of ionomycin. In contrast, cells in control groups without drug stimulation only showed a small decrease in fluorescence intensity within 30 min, and no significant morphological changes were observed (Fig. 4a and b). According to these results, we can infer that a potential correlation may exist between mitochondrial K^+ efflux and early-stage apoptosis.

Furthermore, while a reactive oxygen species (ROS)-induced apoptosis has been indicated to trigger a large amount of potassium ions flowing out of the cytoplasm,[21] levels of K^+ in mitochondria during apoptosis have remained undetermined in real time owing to the lack of organelle-specific K^+ sensors. Since **TAC-Rh** was determined to be an excellent mitochondria-targeting fluorescent K^+ sensor, we further applied it to real-time monitoring of mitochondrial K^+ changes in the H_2O_2-induced apoptotic model. The results showed that compared with the control group (without H_2O_2), the cells of the H_2O_2-treated group were shriveled and the green fluorescence of FITC generally increased; meanwhile, the intensity of the overall red fluorescence of **TAC-Rh** declined gradually, indicating the ability of the apoptosis induced by H_2O_2 to trigger mitochondrial potassium ion efflux (Fig. S20, ESI†). This was the first time that mitochondrial K^+ has been imaged in real time during the process of apoptosis.

As a high concentration of extracellular K^+ can reduce apoptosis and prolong survival of some cells by decreasing the [K^+] gradient between the inside and outside of cells,[22] achieving a delayed apoptosis by increasing the concentration of extracellular K^+ was further carried out. As can be seen in Fig. S21 (ESI†), in contrast to the noticeable weakening of the fluorescence of **TAC-Rh** and the obvious strengthening of FITC signals in the normal culture medium within 8 min of ionomycin stimulation, negligible small changes were observed in the red fluorescence of **TAC-Rh** and the green fluorescence of FITC as well as in the

Open Access Article. Published on 14 April 2020. Downloaded on 12/4/2025 8:25:43 PM.
This article is licensed under a Creative Commons Attribution-NonCommercial 3.0 Unported Licence.

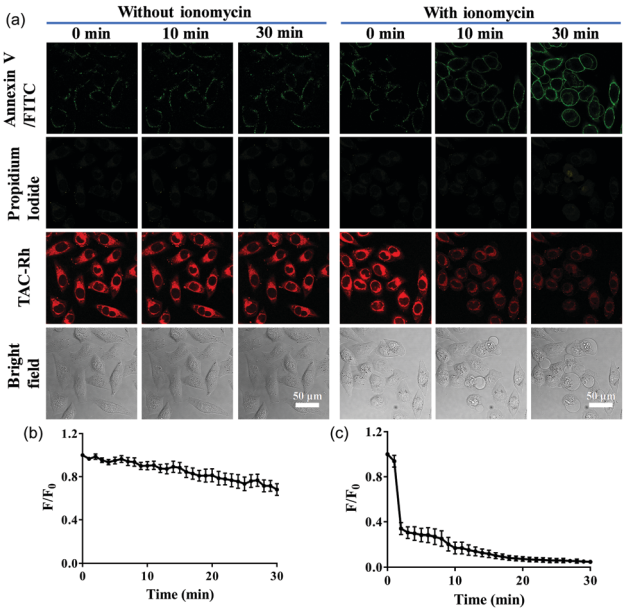

Fig. 4 Time-dependent confocal fluorescence microscopy images of HeLa cells stimulated without and with ionomycin (20 mM) into culture medium stained with annexin V/FITC, propidium Iodide and **TAC-Rh** (a). Average fluorescence intensity ratio (*i.e.*, F/F_0) values of **TAC-Rh** without ionomycin (b) and with ionomycin (c) as measured using Image J, with F_0 denoting the average fluorescence intensity at t = 0 min, and F the average fluorescence intensity at a given time point. Excitation filter: 488 nm for annexin V/FITC, 552 nm for PI, 638 nm for **TAC-Rh**; emission: 493–540 nm for annexin V/FITC, 600–650 nm for PI, 650–750 nm for **TAC-Rh**.

cell morphology in medium containing 80 mM KCl. These phenomena demonstrated that high concentrations of extracellular K^+ could simultaneously inhibit the outflow of K^+ from mitochondria as well as early-stage apoptosis.

In summary, we have developed the first mitochondria-targeting NIR fluorescence K^+ sensor (**TAC-Rh**) by integrating a NIR rhodamine analog with the K^+-binding group TAC. The fluorescence intensity of **TAC-Rh** showed an excellent [K^+]-dependent response and a linear relationship with log[K^+] in the [K^+] range 16–400 mM, features suitable for detecting changes in mitochondria K^+ concentration. The large Stokes shift and NIR emission of **TAC-Rh** minimized the photo-bleaching, light-induced injury, and interference by hemoglobin oxygenation and the cellular fluorescence background. Due to these excellent performance measures, **TAC-Rh** was found to be an excellent material to explore mutual regulation between mitochondrial K^+ flux and apoptosis. This study indicated that (1) HeLa cells treated with ionomycin could result in excessive mitochondrial K^+ efflux accompanied by apoptosis, (2) H_2O_2-induced apoptosis would trigger a large amount of K^+ flux out of mitochondria, and (3) ionomycin-induced mitochondrial K^+ efflux and apoptosis could be inhibited by increasing the K^+ concentration in culture medium. Therefore, **TAC-Rh** was shown to offer a novel strategy to understand mitochondrial K^+ changes during apoptosis, and further investigations using **TAC-Rh** would help researchers derive more information about apoptosis.

The authors would like to thank the National Natural Science Foundation of China (21774054, 21574061), the Shenzhen fundamental research programs (JCYJ20170412152922553), the Macao Science and Technology Development Fund (083/2017/A2), and the Research Fund of the University of Macau (MYRG2016-00130-ICMS-QRCM, MYRG2017-00182-ICMS).

Conflicts of interest

There are no conflicts to declare.

Notes and references

1 C. M. Lopez, A. E. Pineiro, N. Nunez, A. M. Avagnina, E. C. Villaamil and O. E. Roses, *Pharmacol. Res.*, 2000, **42**, 599.
2 S. P. Yu, C. H. Yeh, S. L. Sensi, B. J. Gwag, L. M. Canzoniero, Z. S. Farhangrazi, H. S. Ying, M. Tian, L. L. Dugan and D. W. Choi, *Science*, 1997, **278**, 114.
3 R. Eil, S. K. Vodnala, D. Clever, C. A. Klebanoff, M. Sukumar, J. H. Pan, D. C. Palmer, A. Gros, T. N. Yamamoto, S. J. Patel, G. C. Guittard, Z. Yu, V. Carbonaro, K. Okkenhaug, D. S. Schrump, W. M. Linehan, R. Roychoudhuri and N. P. Restifo, *Nature*, 2016, **537**, 539.
4 S. K. Vodnala, R. Eil, R. J. Kishton, M. Sukumar, T. N. Yamamoto, N. H. Ha, P. H. Lee, M. Shin, S. J. Patel, Z. Yu, D. C. Palmer, M. J. Kruhlak, X. Liu, J. W. Locasale, J. Huang, R. Roychoudhuri, T. Finkel, C. A. Klebanoff and N. P. Restifo, *Science*, 2019, **363**, 135.
5 R. A. J. B. S. Gottlieb, *Receptors*, 2001, **10**, 147.
6 C. Brenner and G. Kroemer, *Science*, 2000, **289**, 1150.
7 R. A. Eliseev, J. D. Salter, K. K. Gunter and T. E. Gunter, *Biochim. Biophys. Acta, Bioenerg.*, 2003, **1604**, 1.
8 (*a*) F. Gottfert, T. Pleiner, J. Heine, V. Westphal, D. Gorlich, S. J. Sahl and S. W. Hell, *Proc. Natl. Acad. Sci. U. S. A.*, 2017, **114**, 2125; (*b*) N. Ji, *Nat. Methods*, 2017, **14**, 374.
9 (*a*) G. Song, R. Sun, J. Du, M. Chen and Y. Tian, *Chem. Commun.*, 2017, **53**, 5602; (*b*) P. Padmawar, X. Yao, O. Bloch, G. T. Manley and A. S. Verkman, *Nat. Methods*, 2005, **2**, 825; (*c*) X. Zhou, F. Su, Y. Tian, C. Youngbull, R. H. Johnson and D. R. Meldrum, *J. Am. Chem. Soc.*, 2011, **133**, 18530; (*d*) B. J. Müller, S. M. Borisov and I. Klimant, *Adv. Funct. Mater.*, 2016, **26**, 7697; (*e*) B. Sui, X. Yue, B. Kim and K. D. Belfield, *ACS Appl. Mater. Interfaces*, 2015, **7**, 17565; (*f*) B. Sui, X. Yue, M. G. Tichy, T. Liu and K. D. Belfield, *Eur. J. Org. Chem.*, 2015, 1189; (*g*) X. Zhou, F. Su, W. Gao, Y. Tian, C. Youngbull, R. H. Johnson and D. R. Meldrum, *Biomaterials*, 2011, **32**, 8574; (*h*) J. Ning and Y. Tian, *Sens. Actuators, B*, 2020, **307**, 127659.
10 S. K. Yao, Y. Qian, Z. Q. Qi, C. G. Lu and Y. P. Cui, *New J. Chem.*, 2017, **41**, 13495.
11 P. Padmawar, X. Yao, O. Bloch, G. T. Manley and A. S. Verkman, *Nat. Methods*, 2005, **2**, 825.
12 X. Kong, F. Su, L. Zhang, J. Yaron, F. Lee, Z. Shi, Y. Tian and D. R. Meldrum, *Angew. Chem., Int. Ed.*, 2015, **54**, 12053.
13 (*a*) J. Li and K. Pu, *Chem. Soc. Rev.*, 2019, **48**, 38; (*b*) D. Wu, L. Chen, W. Lee, G. Ko, J. Yin and J. Yoon, *Coord. Chem. Rev.*, 2018, **354**, 74; (*c*) G. Hong, A. L. Antaris and H. Dai, *Nat. Biomed. Eng.*, 2017, 1.
14 (*a*) W. Namkung, P. Padmawar, A. D. Mills and A. S. Verkman, *J. Am. Chem. Soc.*, 2008, **130**, 7794; (*b*) M. Baruah, W. Qin, R. A. Vallee, D. Beljonne, T. Rohand, W. Dehaen and N. Boens, *Org. Lett.*, 2005, **7**, 4377.
15 H. He, M. A. Mortellaro, M. J. P. Leiner, R. J. Fraatz and J. K. Tusa, *J. Am. Chem. Soc.*, 2003, **125**, 1468.
16 R. D. Carpenter and A. S. Verkman, *Eur. J. Org. Chem.*, 2011, 1242.
17 H. M. D. Bandara, Z. Hua, M. Zhang, S. M. Pauff, S. C. Miller, E. A. C. Davie and W. R. Kobertz, *J. Org. Chem.*, 2017, **82**, 8199.
18 (*a*) J. Li, D. Yim, W. D. Jang and J. Yoon, *Chem. Soc. Rev.*, 2017, **46**, 2437; (*b*) J. Yin, Y. Hu and J. Yoon, *Chem. Soc. Rev.*, 2015, **44**, 4619.
19 W. Xu, Z. Zeng, J. H. Jiang, Y. T. Chang and L. J. A. C. Yuan, *Angew. Chem., Int. Ed.*, 2016, **55**, 13658.
20 S. R. D'Mello, C. Galli, T. Ciotti and P. Calissano, *Proc. Natl. Acad. Sci. U. S. A.*, 1993, **90**, 10989.
21 C. C. Vu, C. D. Bortner and J. A. Cidlowski, *J. Biol. Chem.*, 2001, **276**, 37602.
22 S. R. D'Mello, C. Galli and T. Ciotti, *Proc. Natl. Acad. Sci. U. S. A.*, 1993, **90**, 10989.

 This journal is © The Royal Society of Chemistry 2020